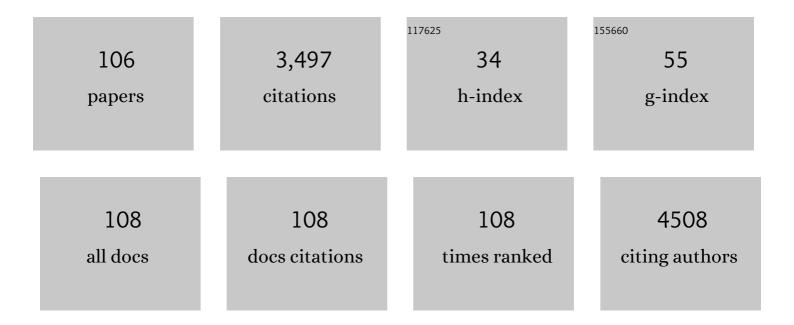
## Ylias M Sabri

List of Publications by Year in descending order

Source: https://exaly.com/author-pdf/2118278/publications.pdf Version: 2024-02-01



#	Article	IF	CITATIONS
1	Recyclable SERS substrate: Optimised by reducing masking effect through colloidal lithography. Applied Surface Science, 2022, 578, 151852.	6.1	6
2	Gold Sunflower Microelectrode Arrays with Dendritic Nanostructures on the Lateral Surfaces for Antireflection and Surface-Enhanced Raman Scattering. ACS Applied Nano Materials, 2022, 5, 1873-1890.	5.0	12
3	Functionalized Concave Cube Cold Nanoparticles as Potent Antimicrobial Agents against Pathogenic Bacteria. ACS Applied Bio Materials, 2022, 5, 492-503.	4.6	11
4	Fabrication of fractal structured soot templated titania-silver nano-surfaces for photocatalysis and SERS sensing. Applied Surface Science, 2022, 594, 153383.	6.1	3
5	Organic ligand interaction with copper(II) ions in both aqueous and non-aqueous media: Overcoming solubility issues for sensing. Sensors and Actuators B: Chemical, 2022, 365, 131934.	7.8	2
6	Reaction mechanism of alkali-activated brick clay mill residues. Construction and Building Materials, 2022, 341, 127817.	7.2	9
7	Enhanced amperometric acetone sensing using electrospun non-stoichiometric WO <sub>3â^'x</sub> nanofibers. Journal of Materials Chemistry C, 2021, 9, 671-678.	5.5	17
8	One-pot conversion of levulinic acid into gamma-valerolactone over a stable Ru tungstosphosphoric acid catalyst. Fuel, 2021, 289, 119900.	6.4	14
9	Band offset in calcium hydroxide mediated CaO-ZnO heterointerfaces. Materials Science and Engineering B: Solid-State Materials for Advanced Technology, 2021, 265, 115005.	3.5	3
10	Treated Municipal Solid Waste (Biomass) Based Concrete Properties—Part I: State of the Art. RILEM Bookseries, 2021, , 295-304.	0.4	1
11	Treated Municipal Solid Waste (Biomass) Based Concrete Properties—Part II: Experimental Program. RILEM Bookseries, 2021, , 281-293.	0.4	1
12	Looking into More Eyes Combining <i>In Situ</i> Spectroscopy in Catalytic Biofuel Upgradation with Composition-Graded Ag–Co Core–Shell Nanoalloys. ACS Sustainable Chemistry and Engineering, 2021, 9, 3750-3767.	6.7	15
13	Liquid Crystal-Mediated 3D Printing Process to Fabricate Nano-Ordered Layered Structures. ACS Applied Materials & Interfaces, 2021, 13, 28627-28638.	8.0	7
14	Microstructural Investigation of High-Volume Fly Ash Composites Containing Nano-Calcium Silicate Hydrate Crystals. Journal of Materials in Civil Engineering, 2021, 33, .	2.9	6
15	Amine-Infused Hydrogels with Nonaqueous Solvents: Facile Platforms to Control CO <sub>2</sub> Capture Performance. Industrial & Engineering Chemistry Research, 2021, 60, 14758-14767.	3.7	7
16	Facile conversion of zinc hydroxide carbonate to CaO-ZnO for selective CO2 gas detection. Journal of Colloid and Interface Science, 2020, 558, 310-322.	9.4	32
17	Mercury in natural gas streams: A review of materials and processes for abatement and remediation. Journal of Hazardous Materials, 2020, 382, 121036.	12.4	49
18	Selective conversion of furfural into tetrahydrofurfuryl alcohol using a heteropoly acid-based material as a hydrogenation catalyst. Sustainable Energy and Fuels, 2020, 4, 4768-4779.	4.9	14

#	Article	IF	CITATIONS
19	Low-Temperature Hydrogen Sensor: Enhanced Performance Enabled through Photoactive Pd-Decorated TiO <sub>2</sub> Colloidal Crystals. ACS Sensors, 2020, 5, 3902-3914.	7.8	41
20	Mercury-bearing wastes: Sources, policies and treatment technologies for mercury recovery and safe disposal. Journal of Environmental Management, 2020, 270, 110945.	7.8	33
21	Electrochemical Evaluation of the Stability and Capacity of râ€GOâ€Wrapped Copper Antimony Chalcogenide Anode for Liâ€Ion battery. ChemElectroChem, 2020, 7, 3291-3300.	3.4	9
22	Leveraging Cu/CuFe <sub>2</sub> O <sub>4</sub> -Catalyzed Biomass-Derived Furfural Hydrodeoxygenation: A Nanoscale Metal–Organic-Framework Template Is the Prime Key. ACS Applied Materials & Interfaces, 2020, 12, 21682-21700.	8.0	75
23	Long-range ordered TiO <sub>2</sub> /Au hollow urchins: topology control for maskless electrodeposition. Journal of Materials Chemistry A, 2020, 8, 26035-26044.	10.3	8
24	Regenerable α-MnO2 nanotubes for elemental mercury removal from natural gas. Fuel Processing Technology, 2019, 193, 317-327.	7.2	53
25	MOF-derived noble-metal-free Cu/CeO <sub>2</sub> with high porosity for the efficient water–gas shift reaction at low temperatures. Catalysis Science and Technology, 2019, 9, 4226-4231.	4.1	25
26	Highly dispersed cobalt oxide nanoparticles on manganese oxide nanotubes for aerobic oxidation of benzyl alcohol. Catalysis Communications, 2019, 130, 105763.	3.3	13
27	Zinc Titanate Nanoarrays with Superior Optoelectrochemical Properties for Chemical Sensing. ACS Applied Materials & Interfaces, 2019, 11, 29255-29267.	8.0	23
28	Co3O4 needles on Au honeycomb as a non-invasive electrochemical biosensor for glucose in saliva. Biosensors and Bioelectronics, 2019, 141, 111479.	10.1	54
29	Inorganic/Organic Heterojunctions: Longâ€Range Ordered Crystals of 3D Inorganic–Organic Heterojunctions via Colloidal Lithography (Small Methods 10/2019). Small Methods, 2019, 3, 1970034.	8.6	0
30	Template based sintering of WO <sub>3</sub> nanoparticles into porous tungsten oxide nanofibers for acetone sensing applications. Journal of Materials Chemistry C, 2019, 7, 2961-2970.	5.5	33
31	Longâ€Range Ordered Crystals of 3D Inorganic–Organic Heterojunctions via Colloidal Lithography. Small Methods, 2019, 3, 1900080.	8.6	8
32	CeO2-Decorated α-MnO2 Nanotubes: A Highly Efficient and Regenerable Sorbent for Elemental Mercury Removal from Natural Gas. Langmuir, 2019, 35, 8246-8256.	3.5	16
33	Transforming Municipal Solid Waste into Construction Materials. Sustainability, 2019, 11, 2661.	3.2	21
34	Functionalization of Elongated Tetrahexahedral Au Nanoparticles and Their Antimicrobial Activity Assay. ACS Applied Materials & Interfaces, 2019, 11, 13450-13459.	8.0	38
35	Cold vapor integrated quartz crystal microbalance (CV-QCM) based detection of mercury ions with gold nanostructures. Sensors and Actuators B: Chemical, 2019, 290, 453-458.	7.8	13
36	Using colloidal lithography to control the formation of gas sorption sites through galvanic replacement reaction. Journal of Colloid and Interface Science, 2019, 547, 199-205.	9.4	1

#	Article	IF	CITATIONS
37	Photo-assisted Amperometric Acetone Sensing of PVP/WO3 Hybrid Nanofibers. , 2019, , .		1
38	Fabrication of a novel ZnIn2S4/g-C3N4/graphene ternary nanocomposite with enhanced charge separation for efficient photocatalytic H2 evolution under solar light illumination. Photochemical and Photobiological Sciences, 2019, 18, 2952-2964.	2.9	36
39	Low-temperature elemental mercury removal over TiO2 nanorods-supported MnOx-FeOx-CrOx. Catalysis Today, 2019, 324, 174-182.	4.4	49
40	Role of Ceria in the Design of Composite Materials for Elemental Mercury Removal. Chemical Record, 2019, 19, 1407-1419.	5.8	19
41	Hybrid Surface and Bulk Resonant Acoustics for Concurrent Actuation and Sensing on a Single Microfluidic Device. Analytical Chemistry, 2018, 90, 5335-5342.	6.5	9
42	Oxygen-deficient photostable Cu <sub>2</sub> O for enhanced visible light photocatalytic activity. Nanoscale, 2018, 10, 6039-6050.	5.6	115
43	Transition (Mn, Fe) and rare earth (La, Pr) metal doped ceria solid solutions for high performance photocatalysis: Effect of metal doping on catalytic activity. Research on Chemical Intermediates, 2018, 44, 2523-2543.	2.7	34
44	SERS and fluorescence-based ultrasensitive detection of mercury in water. Biosensors and Bioelectronics, 2018, 100, 556-564.	10.1	155
45	Silicon as a ubiquitous contaminant in graphene derivatives with significant impact on device performance. Nature Communications, 2018, 9, 5070.	12.8	42
46	Gas sensing performance enhancement: Determining the role of active sites through colloidal lithography. Sensors and Actuators B: Chemical, 2018, 273, 1376-1384.	7.8	5
47	Straddled Band Aligned CuO/BaTiO <sub>3</sub> Heterostructures: Role of Energetics at Nanointerface in Improving Photocatalytic and CO <sub>2</sub> Sensing Performance. ACS Applied Nano Materials, 2018, 1, 3375-3388.	5.0	27
48	Soot template TiO2 fractals as a photoactive gas sensor for acetone detection. Sensors and Actuators B: Chemical, 2018, 275, 215-222.	7.8	66
49	Nano-engineered surfaces for mercury vapor sensing: Current state and future possibilities. TrAC - Trends in Analytical Chemistry, 2017, 88, 77-99.	11.4	29
50	Studying the effect of dealloying Cu-Au nanostructures on their mercury sensing performance. Sensors and Actuators B: Chemical, 2017, 245, 273-281.	7.8	12
51	Easy, one-step synthesis of CdTe quantum dots via microwave irradiation for fingerprinting application. Materials Research Bulletin, 2017, 90, 260-265.	5.2	21
52	Hydrogen sensors based on 2D WO3 nanosheets prepared by anodization. Sensors and Actuators B: Chemical, 2017, 251, 57-64.	7.8	78
53	Galvanic replacement of colloidal monolayer crystal on a QCM device for selective detection of mercury vapor. Sensors and Actuators B: Chemical, 2017, 250, 383-392.	7.8	11
54	Defining the role of humidity in the ambient degradation of few-layer black phosphorus. 2D Materials, 2017, 4, 015025.	4.4	110

#	Article	IF	CITATIONS
55	Nickel–gold bimetallic monolayer colloidal crystals fabricated via galvanic replacement as a highly sensitive electrochemical sensor. Journal of Materials Chemistry B, 2017, 5, 5441-5449.	5.8	8
56	Laying Waste to Mercury: Inexpensive Sorbents Made from Sulfur and Recycled Cooking Oils. Chemistry - A European Journal, 2017, 23, 16219-16230.	3.3	185
57	1,4-Dihydropyrrolo[3,2- <i>b</i> ]pyrroles as a Single Component Photoactive Layer: A New Paradigm for Broadband Detection. ACS Applied Materials & Interfaces, 2017, 9, 27875-27882.	8.0	18
58	Quasi physisorptive two dimensional tungsten oxide nanosheets with extraordinary sensitivity and selectivity to NO <sub>2</sub> . Nanoscale, 2017, 9, 19162-19175.	5.6	81
59	Au Nanospikes as a Nonâ€enzymatic Glucose Sensor: Exploring Morphological Changes with the Elaborated Chronoamperometric Method. Electroanalysis, 2017, 29, 294-304.	2.9	13
60	Detection of alkali emissions from alumina refining processes. Hydrometallurgy, 2017, 170, 68-73.	4.3	0
61	Investigating the cross-interference effects of alumina refinery process gas species on a SAW based mercury vapor sensor. Hydrometallurgy, 2017, 170, 51-57.	4.3	13
62	Efficient Heterostructures of Ag@CuO/BaTiO <sub>3</sub> for Low-Temperature CO <sub>2</sub> Gas Detection: Assessing the Role of Nanointerfaces during Sensing by Operando DRIFTS Technique. ACS Applied Materials & Interfaces, 2017, 9, 27014-27026.	8.0	63
63	A silver electrode based surface acoustic wave (SAW) mercury vapor sensor: a physio-chemical and analytical investigation. RSC Advances, 2016, 6, 36362-36372.	3.6	14
64	Preferential synthesis of highly conducting Tl(TCNQ) phase II nanorod networks via electrochemically driven TCNQ/Tl(TCNQ) solid-solid phase transformation. Journal of Solid State Electrochemistry, 2016, 20, 3303-3314.	2.5	4
65	A nanoengineered surface acoustic wave device for analysis of mercury in gas phase. Sensors and Actuators B: Chemical, 2016, 234, 562-572.	7.8	9
66	Development and experimental verification of a finite element method for accurate analysis of a surface acoustic wave device. Smart Materials and Structures, 2016, 25, 035040.	3.5	17
67	Fe-doped CeO <sub>2</sub> nanorods for enhanced peroxidase-like activity and their application towards glucose detection. Journal of Materials Chemistry B, 2016, 4, 3874-3885.	5.8	151
68	A QCM-based â€~on–off' mechanistic study of gas adsorption by plasmid DNA and DNA–[Bmim][PF6] construct. RSC Advances, 2016, 6, 81318-81329.	3.6	3
69	Hydrogen Bubble Templated Growth of Honeycomb-Like Au-Pt Alloy Films for Non-Enzymatic Glucose Sensing. Journal of the Electrochemical Society, 2016, 163, B689-B695.	2.9	15
70	A real-time comparison of mercury accumulation on noble metal thin films using gravimetric device. Superlattices and Microstructures, 2016, 100, 1151-1158.	3.1	0
71	Mercury Detection in Real Industrial Flue Gas Using a Nanostructured Quartz Crystal Microbalance. Industrial & Engineering Chemistry Research, 2016, 55, 7661-7668.	3.7	5
72	Ordered Monolayer Gold Nano-urchin Structures and Their Size Induced Control for High Gas Sensing Performance. Scientific Reports, 2016, 6, 24625.	3.3	47

#	Article	IF	CITATIONS
73	Candle-Soot Derived Photoactive and Superamphiphobic Fractal Titania Electrode. Chemistry of Materials, 2016, 28, 7919-7927.	6.7	36
74	Development and comparative investigation of Ag-sensitive layer based SAW and QCM sensors for mercury sensing applications. Analyst, The, 2016, 141, 2463-2473.	3.5	18
75	A Nanoengineered Conductometric Device for Accurate Analysis of Elemental Mercury Vapor. Environmental Science & Technology, 2016, 50, 1384-1392.	10.0	20
76	Ceria–zirconia modified MnO <sub>x</sub> catalysts for gaseous elemental mercury oxidation and adsorption. Catalysis Science and Technology, 2016, 6, 1792-1803.	4.1	122
77	Determining the Optimum Exposure and Recovery Periods for Efficient Operation of a QCM Based Elemental Mercury Vapor Sensor. Journal of Sensors, 2015, 2015, 1-7.	1.1	6
78	Selective detection of elemental mercury vapor using a surface acoustic wave (SAW) sensor. Analyst, The, 2015, 140, 5508-5517.	3.5	41
79	Simultaneous multi-mode analysis of surface acoustic wave device temperature stability utilizing time-frequency methods. , 2015, , .		0
80	Nanosphere Monolayer on a Transducer for Enhanced Detection of Gaseous Heavy Metal. ACS Applied Materials & Interfaces, 2015, 7, 1491-1499.	8.0	40
81	Cross sensitivity effects of volatile organic compounds on a SAW-based elemental mercury vapor sensor. Sensors and Actuators B: Chemical, 2015, 212, 235-241.	7.8	12
82	Controlling Core/Shell Formation of Nanocubic <i>p</i> -Cu <sub>2</sub> 0/ <i>n</i> -ZnO Toward Enhanced Photocatalytic Performance. Langmuir, 2015, 31, 10922-10930.	3.5	75
83	Studying mercury partition in monoethylene glycol (MEG) used in gas facilities. Fuel, 2015, 159, 917-924.	6.4	10
84	Mercury Sorption and Desorption on Gold: A Comparative Analysis of Surface Acoustic Wave and Quartz Crystal Microbalance-Based Sensors. Langmuir, 2015, 31, 8519-8529.	3.5	43
85	Catalytic oxidation and adsorption of elemental mercury over nanostructured CeO <sub>2</sub> –MnO <sub>x</sub> catalyst. RSC Advances, 2015, 5, 30331-30341.	3.6	82
86	Highly efficient nanosized Mn and Fe codoped ceria-based solid solutions for elemental mercury removal at low flue gas temperatures. Catalysis Science and Technology, 2015, 5, 2913-2924.	4.1	86
87	Mercury Migration and Speciation Study during Monoethylene Glycol Regeneration Processes. Industrial & Engineering Chemistry Research, 2015, 54, 5349-5355.	3.7	9
88	Silver/gold core/shell nanowire monolayer on a QCM microsensor for enhanced mercury detection. RSC Advances, 2015, 5, 92303-92311.	3.6	18
89	Detect, Remove and Reuse: A New Paradigm in Sensing and Removal of Hg (II) from Wastewater via SERS-Active ZnO/Ag Nanoarrays. Environmental Science & Technology, 2015, 49, 1578-1584.	10.0	122
90	Galvanically replaced Au–Pd nanostructures: study of their enhanced elemental mercury sorption capacity over gold. Physical Chemistry Chemical Physics, 2014, 16, 19522.	2.8	34

#	Article	IF	CITATIONS
91	Gold nanospikes based microsensor as a highly accurate mercury emission monitoring system. Scientific Reports, 2014, 4, 6741.	3.3	44
92	Support Layer Influencing Sticking Probability: Enhancement of Mercury Sorption Capacity of Gold. Journal of Physical Chemistry C, 2013, 117, 8269-8275.	3.1	11
93	Probing the effect of charge transfer enhancement in off resonance mode SERS via conjugation of the probe dye between silver nanoparticles and metal substrates. Physical Chemistry Chemical Physics, 2013, 15, 12920.	2.8	77
94	Structural characterization and catalytic evaluation of transition and rare earth metal doped ceria-based solid solutions for elemental mercury oxidation. RSC Advances, 2013, 3, 12963.	3.6	73
95	Investigation of Hg sorption and diffusion behavior on ultra-thin films of gold using QCM response analysis and SIMS depth profiling. Journal of Materials Chemistry, 2012, 22, 20929.	6.7	12
96	Mercury vapor sensor enhancement by nanostructured gold deposited on nickel surfaces using galvanic replacement reactions. Journal of Materials Chemistry, 2012, 22, 21395.	6.7	33
97	Study of Surface Morphology Effects on Hg Sorption–Desorption Kinetics on Gold Thin-Films. Journal of Physical Chemistry C, 2012, 116, 2483-2492.	3.1	28
98	QCM based mercury vapor sensor modified with polypyrrole supported palladium. Sensors and Actuators B: Chemical, 2011, 160, 616-622.	7.8	28
99	Creating gold nanoprisms directly on quartz crystal microbalance electrodes for mercury vapor sensing. Nanotechnology, 2011, 22, 305501.	2.6	40
100	Mercury diffusion in gold and silver thin film electrodes on quartz crystal microbalance sensors. Sensors and Actuators B: Chemical, 2009, 137, 246-252.	7.8	36
101	In-depth nano-scale analysis of complex interactions of Hg with gold nanostructures using AFM-based power spectrum density method. Physical Chemistry Chemical Physics, 2009, 11, 2374.	2.8	24
102	Gold nanospikes formed through a simple electrochemical route with high electrocatalytic and surface enhanced Raman scattering activity. Chemical Communications, 2009, , 5039.	4.1	90
103	Premonolayer Oxidation of Nanostructured Gold: An Important Factor Influencing Electrocatalytic Activity. Langmuir, 2009, 25, 3845-3852.	3.5	74
104	Electro-deposition of gold nano-structures on gold Quartz Crystal Microbalance (QCM) electrodes for enhanced mercury vapour sensitivity in the presence of interferent gases. , 2008, , .		1
105	Development of nanostructured titanium oxide thin films using a gas carving technique. , 2006, , .		0
106	Gold nanorod self-assembly on a quartz crystal microbalance: an enhanced mercury vapor sensor. Environmental Science: Nano, 0, , .	4.3	1